

Resolving the Parsec-scale Feeding and Feedback Flows of Ionized Gas around Active Galactic Nuclei

Takuma Izumi,^{1,2}

¹*National Astronomical Observatory of Japan, 2-21-1 Osawa, Mitaka, Tokyo 181-8588, Japan*

²*Department of Astronomical Science, The Graduate University for Advanced Studies, SOKENDAI, 2-21-1 Osawa, Mitaka, Tokyo
takuma.izumi@nao.ac.jp*

Abstract

Recent high resolution cold molecular/atomic gas observations have started to reveal detailed spatial structures and dynamics of ~ 100 pc-scale circumnuclear disks (CNDs) around active galactic nuclei (AGNs). In order to extend such efforts to further inner regions around supermassive black holes, where gas is primarily ionized due to the harsh AGN radiation, we here investigate the detectability of mm-HI recombination lines (RLs) with the New Generation Very Large Array (ngVLA). We found that subparsec-scale dense inflows (density $n_e \sim 10^6$ cm $^{-3}$, temperature $T_e \sim 2 \times 10^4$ K) are readily detectable with a reasonable on-source observing time ($\lesssim 10$ hr), allowing us to study detailed spatial distributions, dynamics, and potentially inflow rates, of ionized gas. Rather diffuser and hotter subparsec-scale outflows ($n_e \sim 10^2$ cm $^{-3}$, $T_e \sim 10^6$ K) are impossible to detect even with ngVLA, but there is still a chance to detect a dense one (on-source time ~ 15 hr), which will tell us spatial/dynamical connections of nuclear ionized winds and surrounding cold material. The proposed experiment here will play a vital role to comprehensively understand the multi-phase nature of AGN feeding and feedback.

Key words: galaxies: active — galaxies: evolution — galaxies: ISM — galaxies: nuclei

1. Introduction

The mass accretion onto a supermassive black hole (SMBH; with a mass of $M_{\text{BH}} \gtrsim 10^6 M_{\odot}$) is commonly ascribed to generate the enormous amount of energy that is observed as an active galactic nucleus (AGN) or a quasar (e.g., Alexander & Hickox 2012). AGN can launch fast nuclear outflows that propagate to the host galaxy-scale, clear out the cold gas, and would eventually quench star-formation (e.g., King & Pounds 2015; Veilleux et al. 2020). This *negative* feedback is incorporated to virtually all cosmological galaxy evolution models to reproduce the tight correlation between M_{BH} and bulge scale properties of galaxies observed at the local universe (Kormendy & Ho 2013 for a review). Hence investigating detailed feeding and feedback mechanisms of AGNs is vital to understand the cosmological evolution of SMBHs and galaxies.

Past observations over all electromagnetic wavelength revealed a multi-phase (i.e., ion, atom, and molecule) and complex nature of circumnuclear gas structures at the central $\lesssim 100$ pc scales of AGN-host galaxies (Figure 1). At the immediate vicinity of an AGN, a highly ionized region of fast moving gas is formed (broad line region = BLR), which is further surrounded by a dusty/gaseous obscuring structure (torus) that determines the optical spectroscopic appearance of the AGN (unification model; Antonucci 1993). A more extended (over tens of parsecs to a few kiloparsecs) narrow line region (= NLR) is illuminated by the AGN, which therefore has a characteristic spectral features (e.g., line ratios) as compared to normally star-forming galaxies (e.g., Baldwin et al. 1981).

Recent high resolution cold molecular gas observations by using the Atacama Large Millimeter/submillimeter Array (ALMA) started to reveal that AGNs are usually embedded in $\sim 10 - 100$ parsec (pc) scale dense molecular gas disks

(circumnuclear disk = CND; e.g., Izumi et al. 2016a, 2018; Imanishi et al. 2018; Combes et al. 2019). This CND can work as a direct reservoir of fuel for the central SMBH. Hence a dense gas flow (= inflow), probably through the mid-plane of the CND, would have triggered the AGN. At the NLR-scale, infrared integral-field spectroscopy detected extended outflows traced by some recombination lines and high-ionization lines including [SiVI], [CavIII] (e.g., Müller-Sánchez et al. 2011). These observational facts are well consistent with recent hydrodynamical simulations (e.g., Wada et al. 2016, 2018), in which multi-phase gas flows are responsible for the complex circumnuclear structures.

2. Limitations of the Past Observations

Given the growing success of ALMA, it should be surely feasible to trace molecular gas flows down to ~ 1 pc-scales of nearby AGNs (see early examples in, e.g., Impellizzeri et al. 2019; Imanishi et al. 2020). However, probing further inward regions of AGNs such as 0.1 pc-scale has a fundamental difficulty. That is, AGNs are in principle powerful sources of X-ray radiation, which easily dissociates and ionizes the surrounding dense cold medium to hot plasma (e.g., Maloney et al. 1996; Namekata et al. 2016). Thus we need to perform *ionized gas* observations to ultimately probe gas *inflows* to the SMBHs. In the case of our Galactic Center, Tsuboi et al. (2017) indeed detected pc-scale ionized gas flows toward the Sgr A* traced by H42 α recombination line and 100 GHz continuum emission.

Regarding the *outflows*, there is ample evidence of fast molecular ones in AGN-host galaxies, most of which are considered to be AGN-driven (e.g., Ciccone et al. 2014; Lutz et al. 2020). The molecular phase carry the bulk outflowing mass among the other gas phases (Fluetsch et al. 2019),

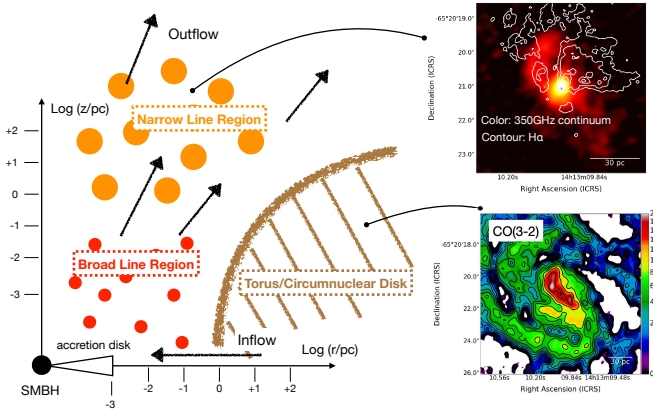


Fig. 1. A schematic view of the circumnuclear gas structures around an AGN (actively mass accreting SMBH). Recent high resolution observations already resolved the structures at $\gtrsim 10$ pc scales: examples of the Circinus galaxy are shown on the right panels (Figures adopted from Izumi et al. 2018). However, the detailed/real structures at $< 0.1 - 1$ pc scales remain unclear: we will tackle this small scale with ngVLA.

which has therefore a crucial impact on galaxy evolution. One possible physical origin of molecular outflows is that the hot, high velocity wind launched from regions close to the AGN hits/accelerates the surrounding molecular clouds of the host galaxy (e.g., Gaspari & Sadowski 2017). However, if the dense molecular gas is settled in a CND and the hot wind is launched to a perpendicular direction relative to this disk (Figure 2), there would be little chance for the hot wind to interact with the surrounding dense gas. In addition, numerical simulations showed that such a hot wind-to-dense gas interaction actually destroys the molecular gas before it is accelerated to the observed outflow velocities of several 100 to 1000 km s^{-1} (e.g., Scannapieco & Brüggen 2015; Schneider & Robertson 2017). An alternative scenario was proposed by Richings & Faucher-Giguère (2018), in which molecules form *in situ* within AGN-driven winds due to efficient radiative cooling. In this case there is probably no need to align high velocity winds and dense gas. To better understand the formation of molecular outflows, observations of the distributions and dynamics of multi-phase winds are therefore essential.

3. High Resolution Mappings of mm-HI Recombination Lines with ngVLA

3.1. Expected Line Flux for Inflows

Considering the background in § 2, we claim that it is imperative to investigate spatial distributions and dynamics of hot ionized gas flows at the close vicinity ($r \lesssim 1$ pc) of AGNs. To this end, mm/submm HI recombination lines (RLs) works powerfully because:

- These lines directly trace ionized gas.
- We can achieve an extraordinary high resolution ($\lesssim 5 - 10$ mas scale) and sensitivity by using ngVLA, which are necessary to probe the very central regions of AGNs.
- Shorter wavelength (e.g., MIR) RLs will suffer a certain amount of dust extinction. Milli-arcsec resolution spectroscopy is impossible at these wavelengths as well.

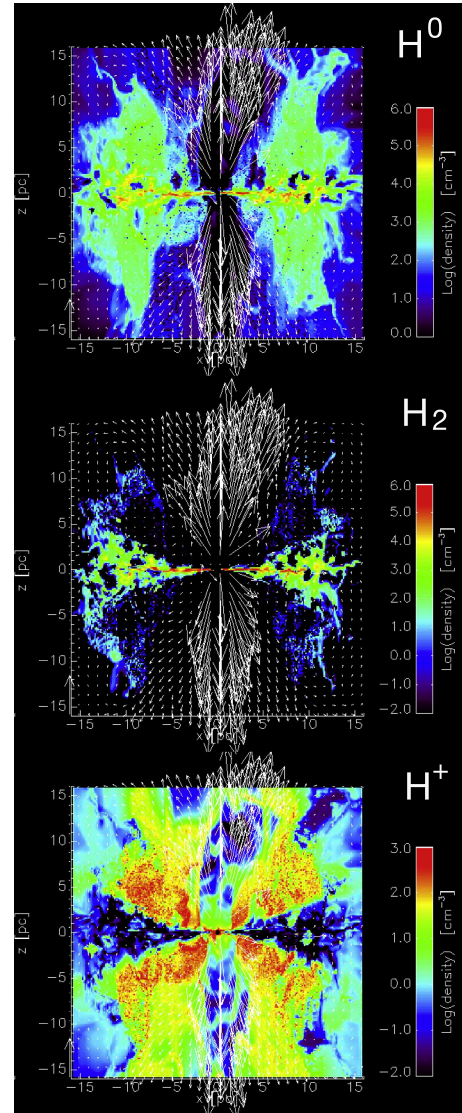


Fig. 2. Simulated distributions of multi-phase gas flows around an AGN ($M_{\text{BH}} = 2 \times 10^6 M_{\odot}$, Eddington ratio = 0.2) adopted from Wada et al. (2016). Colors indicate the gas volume density and the arrows represent velocity vectors of the flows. Each phase gas occupies a different volume. In this simulation, high velocity winds are only visible in the ionized phase, which travel almost perpendicular to the molecular disk.

Table 1. Assumed Conditions for Inflows

Target Line	H42 α (at 85.69 GHz)
$n_e = n_p$ (cm $^{-3}$)	10 6
T_e (K)	2×10^4
l.o.s. Pass Length (pc)	0.05
Line width (FWHM, km s $^{-1}$)	100
He $^+$ /H $^+$ abundance ratio	0.08

- Longer wavelength (cm) RLs will easily become optically thick and sometimes suffer maser amplification. These will simply complicate the situation.

We first investigate a detectability of mm RLs in (sub)pc-scale *inflows* by focusing on H42 α at $\nu_{\text{rest}} = 85.69$ GHz as a representative example. Results can be applied to other RLs with comparable principal quantum numbers.

We now consider physical conditions summarized in Table 1. The electron density (which is identical to the proton density under the fully ionized condition) is set to $n_e = 10^6$ cm $^{-3}$, and the electron temperature is set to $T_e = 2 \times 10^4$ K. These are characteristic to a relatively high density (mid-plane) region of a CND at $r \lesssim 1$ pc as found in very high resolution hydrodynamic simulations of Namekata & Umemura (2016). The line-of-sight (l.o.s.) length of this dense part measured from the face-on angle is ~ 0.05 pc. Although Namekata & Umemura (2016) revealed a geometrically much thicker volume of ionized gas (height ~ 1 pc) with a considerably higher T_e of $\sim 10^{6-7}$ K, we neglect this volume as a simulated gas density there is much smaller (< 100 cm $^{-3}$), which therefore only has a minor contribution to a line intensity. For the case of $(n_e, T_e) = (10^6$ cm $^{-3}$, 2×10^4 K), a departure from the local thermodynamic equilibrium (LTE) should be negligible for a RL with a principal quantum number of $\gtrsim 40$ (Walmsley 1990). Hence we can easily compute the line intensity (brightness temperature unit) by using the l.o.s. emission measure (EM) and a line opacity, which are expressed as:

$$EM \equiv \int \left(\frac{n_e}{\text{cm}^{-3}} \right) \left(\frac{n_p}{\text{cm}^{-3}} \right) \left(\frac{dl}{\text{pc}} \right) \quad (1)$$

$$\tau_{RL} = 1.92 \times 10^3 \left(\frac{T_e}{\text{K}} \right)^{-5/2} \left(\frac{EM}{\text{cm}^{-6} \text{ pc}} \right) \left(\frac{\Delta\nu}{\text{kHz}} \right)^{-1} \quad (2)$$

where $\Delta\nu$ accounts for the line width (100 km s $^{-1} = 28583$ kHz). With the numbers in Table 1, we obtain $\tau_{RL} = 0.059$.

However, we should also consider the underlying free-free continuum emission as this is also emitted from the same gas volume where the line emission originates. By using an appropriate Gaunt factor for free-free transitions, a continuum opacity can be expressed as

$$\tau_C = 8.235 \times 10^{-2} \left(\frac{T_e}{\text{K}} \right)^{-1.35} \left(\frac{\nu}{\text{GHz}} \right)^{-2.1} \left(\frac{EM}{\text{cm}^{-6} \text{ pc}} \right) \quad (3)$$

Note that this continuum EM includes a contribution from He $^+$ ion, which is not the case for H I RLs. This time we obtain a moderate opacity of $\tau_C = 0.606$.

With the above quantities, we can compute the RL intensity and the continuum intensity as

Table 2. Assumed Conditions for Outflows

Target Line	H42 α (at 85.69 GHz)
$n_e = n_p$ (cm $^{-3}$)	10 2
T_e (K)	10 6
l.o.s. Pass Length (pc)	1.0
Line width (FWHM, km s $^{-1}$)	300
He $^+$ /H $^+$ abundance ratio	0.08

Table 3. Assumed Conditions for Very Dense Outflows

Target Line	H42 α (at 85.69 GHz)
$n_e = n_p$ (cm $^{-3}$)	10 4
T_e (K)	2×10^4
l.o.s. Pass Length (pc)	1.0
Line width (FWHM, km s $^{-1}$)	300
He $^+$ /H $^+$ abundance ratio	0.08

$$T_{RL} = T_e (1 - e^{-(\tau_{RL} + \tau_C)}) \quad (4)$$

$$T_C = T_e (1 - e^{-\tau_C}), \quad (5)$$

whereas a *continuum-subtracted* line intensity as

$$\Delta T_{RL} = T_{RL} - T_C \quad (6)$$

For the case of H42 α we now obtain $\Delta T_{RL} \simeq 630$ K. This is fairly a high value thanks to the high T_e and modest opacities explored here. Note that Eq.(6) indicates that no RL can be observed if the continuum emission is heavily optically thick. This is particularly the case for BLR clouds, in which we expect a tremendously high gas density of $n_e \gtrsim 10^{10}$ cm $^{-3}$ (see also Izumi et al. 2016b).

3.2. Expected Line Flux for Outflows

We next consider the (sub)pc-scale outflows by assuming the physical condition in Table 2. The electron density and temperature are the characteristic ones found at several pc-scale extended windy regions in hydrodynamic simulations of Wada et al. (2016). With these numbers, however, we found that both the RL and the underlying free-free continuum are extremely optically thin ($\tau \ll 10^{-9}$), which results in an emergent line flux of almost zero. This is therefore not detectable at all even with ngVLA. Possible exception is very dense outflows (e.g., Kawaguchi et al. 2018) such as $(n_e, T_e) = (10^4$ cm $^{-3}$, 2×10^4 K; Table 3), although simulations usually do not find such dense ionized outflows at the central pc-scales of galaxies. Nevertheless, in this case we expect a line intensity of $\Delta T_{RL} \sim 1$ K.

3.3. High-resolution Observations with ngVLA

Given the brightness, we first consider requirements (resolution, sensitivity, etc.) for *inflow* observations. Tsuboi et al. (2017) mapped H42 α distribution around Sgr A* (Figure 3), which revealed spiral flows with a length of ~ 1.5 pc and a width of $\sim 0.2 - 0.3$ pc. Therefore, we request spatial resolutions better than 0.3 pc for our study so that we can spatially resolve the ionized inflows in nearby AGNs. Note that it is

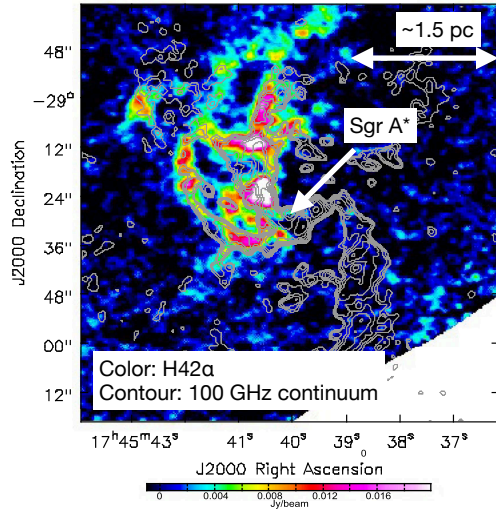


Fig. 3. Velocity channel map (80 km s^{-1}) of the Galactic Center region traced by the H42 α recombination line (color), overlaid with the 100 GHz continuum emission contours (adopted from Tsuboi et al. 2017). One can identify spiral flows of ionized gas with a spatial extent of $\sim 1.5 \text{ pc}$, traveling down to the Sgr A*.

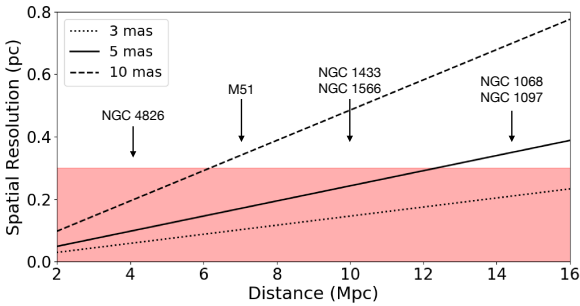


Fig. 4. Expected physical resolutions for three example ngVLA angular resolutions (3, 5, and 10 mas) as a function of the distance to the target galaxy. The shade region indicates our acceptable resolution range (i.e., $\lesssim 0.3 \text{ pc}$) to properly map ionized flows (see also Figure 3). Some famous AGNs observable from ngVLA are marked.

also plausible that AGNs have more extended ionized flows ($\gg 1 \text{ pc}$) given the fact that Sgr A* is a much less active system than typical Seyfert galaxies by orders of magnitude: in this case we can readily resolve the flows by the 0.3 pc resolution. We show in Figure 4 this spatial resolution limit as a function of the distance (D) to a target galaxy. Thanks to the extremely high angular resolutions ($< 10 \text{ mas}$) provided by ngVLA, we can surely fulfill this resolution requirement up to $D \sim 15 \text{ Mpc}$. Note that this cosmic volume includes some representative AGNs in the nearby universe such as NGC 1068, NGC 1097, and M51.

For example, suppose M51 as our fiducial target AGN (Table 4), which is located at $D \sim 7 \text{ Mpc}$. Due to this proximity, we can obtain, e.g., 0.2 pc resolution with a 5.8 mas beam. According to the ngVLA Key Performance Metrics, we will obtain 1σ sensitivity of 60 K with only $\sim 7.5 \text{ hr}$ on-source integration. This allows a $\sim 10\sigma$ detection of the ΔT_{RL} of H42 α (line center). This high S/N should be sufficient to map the gas

Table 4. Fiducial Feasibility Estimation (M51; inflow)

Physical Resolution	0.2 pc
Angular Resolution	5.8 mas ($D = 7 \text{ Mpc}$)
Velocity Resolution	10 km s^{-1}
Targeted 1σ	60 K
On-source time	$\sim 7.5 \text{ hr}$

distributions in detail, as well as to assess ionized gas dynamics there with dynamical modelings that isolate non-circular motions from rotation + random dispersion motions. We can therefore answer some key questions including:

- Can we see spiral flows like those in Sgr A*?
- Can we see non-axisymmetric gas distribution at the final pc-scale region, which is essential to cause gravitational instability?
- What is the spatial connection of these ionized flows to the larger scale cold gas distributions probed by, e.g., ALMA?
- What is the 3D geometry of the flows? We can constrain this (scale height/length ratio = aspect ratio) from the decomposed dispersion-to-rotation velocity ratio.
- How fast are the inflows?
- What is the inflow rate ($\equiv \dot{M}$)?

Note that the flux of RLs depends on the line emissivity and EM as long as the emission is (at least moderately) optically thin. Here the line emissivity is almost independent of n_e for RLs considered here (Scoville & Murchikova 2013). That is, once we constrain the 3D geometry, we can roughly compute n_e from EM, which would deliver the 1st-order estimation of \dot{M} when combined with information of the spatial structure and the inflow velocity. The proposed observation here will finally bridge the innermost part of a molecular CND and a BLR/accretion disk scale, enabling a thorough discussion on dynamical gas flows at the central $< 10 \text{ pc}$ scales of AGNs.

For the case of *vey dense outflows* (Table 3), it is still not practical to request mas-scale resolutions, which will inflate the observational time. Even for ngVLA, this experiment is only feasible for rather modest angular resolutions of $\gtrsim 0''.1$, which corresponds to $\gtrsim 3.4 \text{ pc}$ at the distance of M51. With this reduced resolution, we may obtain $\sim 10\sigma$ detection of the outflowing H42 α with a $\sim 15 \text{ hr}$ on-source time ($dV = 30 \text{ km s}^{-1}$). This is still worth doing to reveal the feedback properties at the central $< 10 \text{ pc}$ regions of AGNs. By assessing the dynamical properties and mapping the intensity distribution, we would like to answer these questions:

- What is the spatial connection of the outflowing ionized gas and the surrounding cold gas?
- In particular, can we see the site at which ionized outflows indeed contact cold molecular/atomic gas?
- Is the outflow velocity sufficiently high to escape from the gravitational potential of the SMBH?

4. Summary

In this article we investigated the detectability of mm H I recombination lines (example case = H42 α) at the close vicinity

(< 1 pc) of AGNs. This is essential to comprehensively understand the feeding and feedback of AGNs, primarily because cold gas (molecule + atom) must be heated and ionized by the central AGN at that innermost part, i.e., cold gas observations cannot probe such core regions in principle. This experiment requires quite high angular resolutions (mas-scale) and sensitivity, which are only achievable by ngVLA.

Regarding the subpc-scale ionized inflows, we found that they are readily detectable in nearby AGNs ($D \lesssim 15$ Mpc). We can therefore investigate detailed ionized gas distributions, dynamics including inflow velocities, inflow rates, as well as physical connections to larger-scale cold gas disks probed by, e.g., ALMA (and ngVLA itself). On the other hand, due to the likely less-dense and hotter nature of the gas therein, it is quite difficult to detect (relatively diffuse) ionized outflows at the central pc-scale region. Ionized outflows would only be detectable if the gas density is sufficiently high and the temperature is modest. Even so, we may be able to investigate a slightly larger scale (< 10 pc) ionized outflow properties, which still has a substantial impact on feedback studies.

References

- Alexander, D. M. & Hickox, R. C., 2012, *New Astronomy Reviews*, 56, 4
- Antonucci, R., 1993, *ARA&A*, 31, 473
- Baldwin, J. A., Phillips, M. M., & Terlevich, R., 1981, *PASP*, 93, 5
- Cicone, C., et al., 2014, *A&A*, 562, A21
- Combes, F., et al., 2019, *A&A*, 623, A79
- Fluetsch, A., et al. 2019, *MNRAS*, 483, 4586
- Gaspari, M., & Sadowski, A., 2017, *ApJ*, 837, 149
- Imanishi, M., et al., 2018, *ApJL*, 853, L25
- Imanishi, M., et al., 2020, *ApJ*, 902, 99
- Impellizzeri, C. M. V., et al., 2019, *ApJL*, 884, L28
- Izumi, T., Kawakatu, N., & Kohno, K., 2016a, *ApJ*, 827, 81
- Izumi, T., et al., 2016b, *MNRAS*, 459, 3629
- Izumi, T., et al., 2018, *ApJ*, 867, 48
- Kawaguchi, T., et al., 2018, *PASJ*, 70, 93
- King, A. & Pounds, K., 2015, *ARA&A*, 53, 115
- Kormendy, J. & Ho, L. C., 2013, *ARA&A*, 51, 511
- Lutz, D., et al., 2020, *A&A*, 633, A134
- Maloney, P. R., Hollenbach, D. J., & Tielens, A. G. G. M., 1996, *ApJ*, 466, 561
- Namekata, D., & Umemura, M., 2016, *MNRAS*, 460, 980
- Muller-Sanchez, F., et al., 2011, *ApJ*, 739, 69
- Richings, A. J., & Faucher-Giguère, C.-A., 2018, *MNRAS*, 474, 3673
- Scannapieco, E., & Brüger, M., 2015, *ApJ*, 805, 158
- Schneider, E. E., & Robertson, B. E., 2017, *ApJ*, 834, 144
- Scoville, N., & Murchikova, L., 2013, *ApJ*, 779, 75
- Tsuboi, M., et al., 2017, *ApJ*, 842, 94
- Veilleux, S., et al., 2020, *A&ARv*, 28, 2
- Wada, K., Schartmann, M., & Meijerink, R., 2016, *ApJL*, 828, L19
- Wada, K., Yonekura, K., & Nagao, T., 2018, *ApJ*, 867, 49
- Walmsley, C. M., 1990, *A&AS*, 82, 201